

Population III Binary Black Holes: Effects of Convective Overshooting on Formation of GW190521

Ataru Tanikawa,^{1,*} Tomoya Kinugawa,² Takashi Yoshida,³ Kotaro Hijikawa,³ Hideyuki Umeda³

¹*Department of Earth Science and Astronomy, College of Arts and Sciences, The University of Tokyo, 3-8-1 Komaba, Meguro-ku, Tokyo 153-8902, Japan*

²*Institute for Cosmic Ray Research, The University of Tokyo, Kashiwa, Chiba, Japan*

³*Department of Astronomy, Graduate School of Science, The University of Tokyo, Bunkyo-ku, Tokyo, Japan*

Accepted XXX. Received YYY; in original form ZZZ

ABSTRACT

GW190521 is a merger of two black holes (BHs), wherein at least one BH lies within the pair-instability (PI) mass gap, and it is difficult to form because of the effects of PI supernovae (PISNe) and pulsational PI (PPI). In this study, we examined the formation of GW190521-like BH-BHs under Population (Pop) III environments by binary population synthesis calculations. We reveal that convective overshooting in stellar evolution strongly affects the formation of GW190521-like BH-BHs. A model with a small overshoot parameter (similar to GENECS) can form GW190521-like BH-BHs. The derived merger rate is $4 \times 10^{-2} \text{ yr}^{-1} \text{ Gpc}^{-3}$ at a redshift of ~ 0.82 , which is comparable to the merger rate of GW190521-like BH-BHs inferred by gravitational wave (GW) observations. In this model, a $\sim 90 M_{\odot}$ star collapses to form a $\sim 90 M_{\odot}$ BH by avoiding PPI and PISN even if it is a member of a binary star. This is because it expands up to $10^2 R_{\odot}$, and lose only little mass through binary evolution. However, a model with a large overshoot parameter (similar to Stern) cannot form GW190521-like BH-BHs at all. Thus, we cannot conclude that a Pop III binary system is the origin of GW190521 because determination of the overshoot parameter involves highly uncertain. If a Pop III binary system is the origin of GW190521, the merger rate of BH-BHs including a $100 - 135 M_{\odot}$ BH is substantially smaller than that of GW190521-like BH-BHs. This will be assessed by GW observations in the near future.

Key words: binaries: close – stars: black holes – stars: Population III – gravitational waves – black hole mergers

1 INTRODUCTION

The first binary black hole (BH-BH) merger was observed in the first direct detection of gravitational waves (GWs) (Abbott et al. 2016). Since then, many BH-BHs have been discovered. By the end of the first and second observing runs (O1 and O2, respectively) 10 BH-BHs were discovered (Abbott et al. 2019a). This number increased by 4 times in the first-half of the third observing run (O3a) (Abbott et al. 2020a; The LIGO Scientific Collaboration et al. 2020). The O3a has not only discovered more BH-BHs, but has also discovered BH-BHs with different properties from those discovered in the O1/O2, such as GW190412 with asymmetric masses (Abbott et al. 2020b) and GW190814 with a compact object in the lower mass gap (MG) (Abbott et al. 2020d).

GW190521 was also discovered in the O3a, which is a BH-BH with a total mass of $150 M_{\odot}$ (Abbott et al. 2020c). The presence of GW190521 is surprising because at least one of the two BHs can be in the pair-instability (PI) MG $65 - 130 M_{\odot}$, which was not discovered in the O1/O2 (Abbott et al. 2019b). This type of BHs are difficult to form because of PI supernovae (SNe) (Barkat et al. 1967; Fraley 1968; Bond et al. 1984; El Eid & Langer 1986; Fryer et al. 2001; Heger & Woosley 2002; Umeda & Nomoto 2002), and pulsational PI (PPI) (Heger & Woosley 2002; Yoshida et al. 2016;

Leung et al. 2019). Many formation scenarios of GW190521 have been summarized by Abbott et al. (2020e): hierarchical BH mergers in globular clusters (Rodriguez et al. 2019), stellar collisions in open clusters (Di Carlo et al. 2020), and combination of BH mergers and gas accretion in disks of active galactic nuclei (Yang et al. 2019; Tagawa et al. 2020; Mapelli et al. 2020a). Gas accretion may bridge the PI MG (Roupas & Kazanas 2019). Fishbach & Holz (2020) have proposed that GW190521 consists of BHs below and above the PI MG. If so, GW190521 can be formed through Population (Pop) I/II and Pop III binary evolutions (Mangiagli et al. 2019; Tanikawa et al. 2021, respectively). An electromagnetic counterpart of GW190521 was actively discussed (Graham et al. 2020; Palmese et al. 2021).

Farrell et al. (2021) (F21) have claimed that Pop III binary systems can form GW190521. This is because Pop III stars lose little mass through stellar winds, keep their stellar radii small so as not to interact with their companion stars, and have small carbon-oxygen (CO) core mass because of H-He shell interactions. This is contrasting to the results obtained by Tanikawa et al. (2021) (T21) in which Pop III binary systems hardly form GW190521-like BH-BHs. T21 have not found the formation of GW190521-like BH-BHs. This discrepancy results from the choice of a convective overshoot parameter for a stellar evolution model. F21 and T21 have adopted small and large overshoot parameters, respectively. If a convective overshoot parameter is small, a Pop III star keeps a small radius until collapse to a BH, loses little mass through binary interaction and can leave BHs in the

* E-mail: tanikawa@ea.c.u-tokyo.ac.jp

PI MG. It is difficult to identify the correct parameters. The overshoot parameter in F21’s model is the same as that in GENEC to explain the main-sequence width of AB stars observed in open clusters in the Milky Way Galaxy (Ekström et al. 2012), while the overshoot parameter in T21’s model is calibrated based on Stern to explain the early B-type stars observed in the Large Magellanic Cloud (Brott et al. 2011).

Kinugawa et al. (2021a) (K21) have suggested that Pop III binary systems can form a large number of GW190521-like BH-BHs, and that the merger rate is comparable to the rate of GW190521, despite that they have adopted a stellar evolution model constructed by Marigo et al. (2001) with similar behaviors to a model with a large convective overshoot parameter. This is because of their modeling of post main-sequence (MS) stellar radii. However, we show that their modeling is not applicable to Pop III stars that form BHs in the PI MG.

In this study, we showed that the choice of convective overshooting parameters strongly affects the formation of GW190521-like BH-BHs from Pop III binary systems. We perform binary population synthesis (BPS) calculations for three stellar models with different convective overshoot parameters. Two of the three models have small and large convective overshoot parameters, and are called the M and L models, respectively (Yoshida et al. 2019). The overshoot parameters of the M and L models are calibrated to GENEC (Ekström et al. 2012) and Stern (Brott et al. 2011), respectively. The M and L models are named after the first letters of the Milky Way galaxy and the Large Magellanic Cloud, whose stars are used for calibrations by GENEC and Stern, respectively. The M model is similar to the F21’s model. The L model is the same as the T21’s model. The third model is the L model with K21’s modeling of post-MS stellar radii, which is similar to the K21’s model.

Liu & Bromm (2020a,b) examined the formation of GW190521-like BH-BHs from Pop III stars through dynamical interactions, and Safarzadeh & Haiman (2020) considered Pop III BH growth via gas accretion. In contrast, we focus on formation of GW190521-like BH-BHs from Pop III binary systems through pure binary evolution. Belczynski (2020) suggested that GW190521-like BH-BHs can be formed from Pop II binary systems through pure binary evolution, if stars with He cores of $90 M_{\odot}$ can avoid PPI and PISNe (Takahashi 2018; Farmer et al. 2020; Costa et al. 2021). This is true only if the $^{12}\text{C}(\alpha, \gamma)^{16}\text{O}$ reaction rate is lower than its standard reaction rate by 3σ . In this study, we assumed that stars with He cores of $45 - 65 M_{\odot}$ experience PPI and leave $45 M_{\odot}$ BHs, and that stars with He cores of $65 - 135 M_{\odot}$ experience PISNe, and leave no remnants. This assumption makes it difficult to form GW190521-like BH-BHs through pure binary evolution; however, it is based on the results of PPI and PISNe with the standard $^{12}\text{C}(\alpha, \gamma)^{16}\text{O}$ reaction rate. Many other formation scenarios have been suggested immediately after the publication of GW190521 (Moffat 2020; Gayathri et al. 2020; Palmese & Conselice 2020; Anagnostou et al. 2020; Sakstein et al. 2020; Fragione et al. 2020; Romero-Shaw et al. 2020; Renzo et al. 2020; Rice & Zhang 2021; Bustillo et al. 2021; De Luca et al. 2021). After submission of this manuscript, we became aware of the complementary work by Vink et al. (2021), which independently finds that uncertainty in convective overshooting leads to significant uncertainty in predictions for the maximum BH mass which can be formed below the PI MG.

The remainder of this paper is structured as follows. In section 2, we present our BSE code and initial conditions. In section 3, we detail the results of the BPS calculations. In section 4, we summarize this study.

2 METHOD

We used a widely-used BPS code BSE (Hurley et al. 2000, 2002) with extensions to massive and extremely metal-poor stars (Tanikawa et al. 2020). Herein, we briefly introduce our BSE code, described in detail in T21 and Tanikawa et al. (2020). We did not account for stellar wind mass loss because of Pop III stars, although our BSE code can include stellar wind mass loss. Figure 1 shows Hertzsprung–Russell (HR) diagram of stars $M_{\text{zams}} = 10 - 160 M_{\odot}$ at intervals of $2^{1/2}$ from bottom to top for the M (blue) and L (red) models. Stars in the M model maintain substantially smaller radii than in the L model. This is because of difference in convective overshoot parameters between these models. In our stellar evolution calculations, convective overshoot is taken with a diffusive treatment. The diffusion coefficient exponentially decreases with the distance from a convection boundary with a scale of $f_{\text{ov}} H_P / 2$, where H_P is the pressure scale height at the boundary. The L model adopts larger convective overshoot parameter ($f_{\text{ov}} = 0.03$) than the M model ($f_{\text{ov}} = 0.01$). When convective overshooting is more effective, post-MS stars have larger He core masses. The larger He cores emit larger luminosities, and the larger luminosities expand the stellar radii more (e.g. Podsiadlowski 1992). In the L model, the star with $M_{\text{zams}} = 80 M_{\odot}$ exceeds $10^3 R_{\odot}$, which is consistent with the results of Marigo et al. (2001) and Yoon et al. (2012). In the M model, the star with $M_{\text{zams}} = 80 M_{\odot}$ expands up to $\sim 40 R_{\odot}$, which is smaller than the radius of the corresponding radius in F21, $\sim 160 R_{\odot}$. Nevertheless, this is rather helpful for the aim of investigating the dependence of GW190521 formation on convective overshooting.

We highlight that the M and L models are not the same as GENEC and Stern, respectively. Yoshida et al. (2019) did not compare their simulation results with observed stars themselves. Instead, they showed that in the solar metallicity the evolutions of $20 M_{\odot}$ stars in the M and L models are comparable to those calculated by the GENEC and Stern codes, respectively. These stars have remarkably higher metallicity than Pop III stars and have much smaller mass than stars forming BHs in PI MG. Moreover, the HOSHI code treats convection differently from the GENEC and Stern codes. Both the Stern and HOSHI codes use the Ledoux criterion for convection; however, they adopt different semiconvection parameters. The GENEC code uses the Schwarzschild criterion for convection. Moreover, the HOSHI code uses an exponential description of convective overshooting, while the GENEC and Stern codes use step-function overshooting descriptions. Thus, the M and L models do not have the same quantitative evolution of $80 M_{\odot}$ stars with zero metallicity as the GENEC and Stern codes, although they have qualitatively the same. We also mention our treatment of stellar surface in the HOSHI code. It is difficult to solve the evolution of the convective envelope with high Eddington factors in massive stars and some numerical treatments are adopted to be solved (Paxton et al. 2013; Sanyal et al. 2017). The different treatments would affect the radial evolution. In this study, we did not adopt any special treatments in the HOSHI code to solve the surface evolution. The surface evolution problem is less serious in Pop III massive stars¹.

For a supernova model, we adopted the rapid model in Fryer et al. (2012) modified by PPI and PISNe. Stars with He core masses of $45 - 65 M_{\odot}$ and $65 - 135 M_{\odot}$ experience PPI and PISNe, respectively. If stars experience PPI and PISNe, they leave $45 M_{\odot}$ BHs and no remnants, respectively, which is similar to a strong PPI model

¹ We limit the opacity so that the local luminosity does not exceed the Eddington luminosity in the region where $M_r > 0.99 M_{\text{total}}$ in case of $Z \geq 0.01 Z_{\odot}$ star.

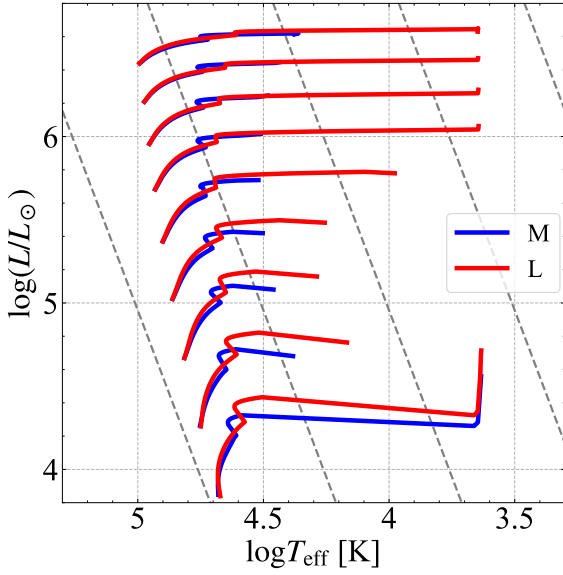


Figure 1. Hertzsprung–Russell (HR) diagram of stars with $M_{\text{zams}} = 10 - 160 M_{\odot}$ at intervals of $2^{1/2}$ from bottom to top for the M (blue) and L (red) models. Gray dashed lines indicate stellar radii of $1 - 10^4 R_{\odot}$ at intervals of 10 from left to right.

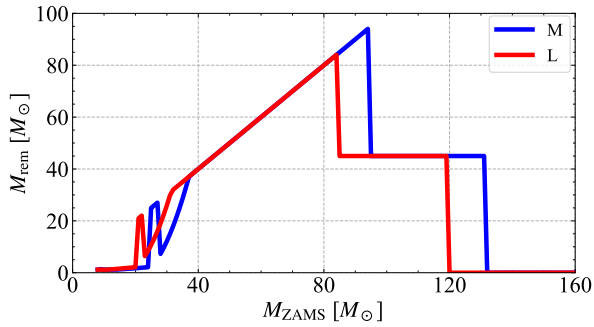


Figure 2. Relation between zero-age main-sequence (ZAMS) and remnant masses in the M and L models.

constructed by [Belczynski et al. \(2016\)](#)². Figure 2 shows the relation between ZAMS and remnant masses in the M and L models. In both the models, stars with $M_{\text{zams}} \sim 90 - 130 M_{\odot}$ leave $45 M_{\odot}$ BHs because of PPI, and stars with $M_{\text{zams}} \geq 130 M_{\odot}$ leave no remnants because of PISNe. Stars with $M_{\text{zams}} \sim 50 - 90 M_{\odot}$ can leave BHs with $\geq 45 M_{\odot}$, because they have small He core mass with $\leq 45 M_{\odot}$, and do not experience PPI nor PISNe. [Mapelli et al. \(2020b\)](#) and [Costa et al. \(2021\)](#) have also predicted BHs with $\geq 45 M_{\odot}$ can be formed through the same mechanism. The L model has lighter ZAMS stars undergoing PPI and PISNe than the M model. This is because stars form larger He cores in the L model than in the M model. Furthermore, we do not consider BH natal kicks.

Our BSE code treats binary interactions similar to the original BSE

code ([Hurley et al. 2002](#)). Here, we describe different points between the original and our BSE code. The original BSE code considers the stars with convective and radiative envelopes as those in the phases of core helium burning and shell helium burning, respectively. In contrast, our BSE code models stars with convective and radiative envelopes as stars with the effective temperature of $< 10^{3.65}$ K and $> 10^{3.65}$ K, respectively. This affects the tidal interactions and mass transfer. In tidal interactions, the equilibrium tide with convective damping is adopted for stars with convective envelopes, while the dynamical tide with radiative damping is adopted for stars with radiative envelopes. In mass transfer, stars with convective envelopes experience unstable mass transfer (common envelope evolution) more easily than those with radiative envelopes. Common envelope evolution is approximated as the α formalism (e.g. [Webbink 1984](#)). We adopt $\alpha_{\text{CE}} \lambda_{\text{CE}} = 1$, where α_{CE} is the common envelope efficiency, and λ_{CE} is the structural binding energy parameter. Furthermore, we consider orbital shrinkage because of GW radiation. We switch off magnetic braking because Pop III binary systems should have only tangled magnetic field ([Sharda et al. 2020](#)).

We prepare 10^6 binary systems for initial conditions. Their distributions of initial primary masses ($m_{1,i}$), mass ratios q_i , semi-major axes (a_i), and eccentricities (e_i) are the same as those of the opt1e1q0.0 model in T21 except for the maximum primary mass. The details are as follows. The distribution of the initial primary mass ($m_{1,i}$) is proportional to $m_{1,i}^{-1}$ in the range of $10 - 150 M_{\odot}$ because the initial mass function of Pop III stars are predicted to be logarithmically flat in the mass range from a few $10 M_{\odot}$ to a few $100 M_{\odot}$ by numerical simulations (e.g. [Susa et al. 2014](#); [Hirano et al. 2014](#)). Pop III stars can have larger masses and our main objective is to form BHs in the PI MG; thus, they are not considered here. The distribution of initial mass ratio q_i is uniform in the range from $10 M_{\odot}/m_{1,i}$ to 1. The distribution of initial semi-major axis (a_i) is logarithmically flat ($\propto a_i^{-1}$) in the range of $10 - 2000 R_{\odot}$. We set the eccentricity distribution to the thermal distribution, $\propto e_i$. We exclude binary systems if at least one of two stars fills its Roche lobe at the initial time.

We applied the M and L models to these binary systems. The M model is similar to the F21’s model, and the L model is the same as the T21’s model. Additionally, we adopt the L model with K21’s modeling of post-MS radii (hereafter, L+K21 model), which is similar to the model of K21. In the L+K21 model, stars evolve along with the L model unless they experience stable mass transfer. Post-MS stars in the L+K21 model respond to mass loss through mass transfer differently from post-MS stars in the L model in the following. Generally, a post-MS star slowly shrinks with mass loss of its hydrogen envelope, and steeply shrinks to its He core size around when it completely loses its hydrogen envelope. Thus, we modeled the response of a post-MS radius to mass loss, such that a post-MS star suddenly shrinks down to its He core size, when a fraction of its He core mass (M_c) to its total mass (M_t) becomes larger than a critical value. Hereafter, we call the critical value $q_{\text{He,crit}}$. In other words, a post-MS star shrinks to its He core size when $M_c/M_t > q_{\text{He,crit}}$. In the M and L models, $q_{\text{He,crit}} \sim 0.99$, which is the same as the SSE/BSE codes (see Appendix A). In contrast, in the L+K21 model, $q_{\text{He,crit}} = 0.58$ ³. This is based on the result of [Inayoshi et al. \(2017\)](#) (see their section 2.2.5). This $q_{\text{He,crit}}$ may be appropriate for Pop III stars with $M_{\text{zams}} = 20 - 50 M_{\odot}$; however, it may not be appropriate

² [Umeda et al. \(2020\)](#) have intensively investigated PPI and PISN of Pop III stars.

³ Actually, K21 have not explicitly described that they have adopted $q_{\text{He,crit}} = 0.58$.

Table 1. Parameters of GW190521 we adopted.

Parameter		
Primary mass	$85^{+21}_{-14} M_{\odot}$	90% credible intervals
Secondary mass	$66^{+17}_{-18} M_{\odot}$	90% credible intervals
Total mass	$150^{+29}_{-17} M_{\odot}$	90% credible intervals
Redshift	$0.82^{+0.28}_{-0.34}$	90% credible intervals
Rate	$0.13^{+0.30}_{-0.11} \text{ yr}^{-1} \text{ Gpc}^{-3}$	

for Pop III stars with $M_{\text{zams}} = 60 - 90 M_{\odot}$, which form BHs in the PI MG (Figure 2). We discuss this in Section 3.

We assumed a simple Pop III star formation model as follows. All Pop III stars are formed in minihalos at the redshift of ~ 10 . All the minihalos form one Pop III binary systems. The number density of minihalos is 10^{11} Gpc^{-3} , and then the number density of Pop III binary systems is 10^{11} Gpc^{-3} . This formation model is consistent with Magg et al. (2019) and Skinner & Wise (2020) with respect to the total Pop III mass in the local universe. In contrast, the total Pop III mass is much smaller than estimated by de Souza et al. (2011) and Inayoshi et al. (2016), which are adopted by Kinugawa et al. (2014, 2020, 2021b), and K21. Our Pop III formation rate may be pessimistically small.

Table 1 presents the parameters of GW190521 we adopted. All parameters (except rate) have error bars of 90% credible intervals. These parameters are detailed by Abbott et al. (2020c) and Abbott et al. (2020e).

3 RESULTS

We define the merger rate density of BH-BHs as follows:

$$\Gamma = \frac{d(N_{\text{BH-BH}}/N_{\text{bin}})}{dt_d} \left(\frac{\eta_{\text{bin}}}{1} \right) \left(\frac{n_{\text{DM}}}{10^{11} \text{ Gpc}^{-3}} \right) [\text{yr}^{-1} \text{ Gpc}^{-3}], \quad (1)$$

where N_{bin} is the number of simulated binary systems, $N_{\text{BH-BH}}$ is the number of merging BH-BHs, t_d is the delay time, η_{bin} is the number of Pop III binary systems formed in each minihalo, and n_{DM} is the number density of the minihalo. Figure 3 shows the merger rate density of BH-BHs in the M, L, and L+K21 models as a function of the delay time. After $\sim 10^2$ Myr, the distributions of all BH-BH merger are similar among the three models. In all the models, these BH-BHs are formed through stable mass transfer. In contrast, the merger rates in the L and L+K21 models are much larger than in the M model before $\sim 10^2$ Myr. Stars expand up to $10^3 R_{\odot}$ and evolve to form red-supergiant stars in the L and L+K21 models; thus, binary stars can experience common envelope evolution. The resulting BH-BHs can have semi-major axes comparable to the size of He cores, and have short GW radiation timescales ($\lesssim 10^2$ Myr). If binary stars do not undergo common envelope evolution, their semi-major axes are at least the size of their ZAMS radii, and then their GW radiation timescales are long, $\gtrsim 10^2$ Myr. In all the models, the merger rates of BH-BHs at ~ 10 Gyr are $\sim 10^{-1} \text{ yr}^{-1}$, which is consistent with T21.

Figure 3 shows the merger rate density of BH-BHs, whose total masses are $150^{+29}_{-17} M_{\odot}$, within the error bar of the total mass of GW190521. There are many such BH-BHs in the M model, while there is no such BH-BH in the L model. In the L model, stars with $M_{\text{zams}} = 50 - 90 M_{\odot}$ expand to $\gtrsim 10^3 R_{\odot}$, and evolve to red-supergiant stars. Such stars interact with their companion stars and

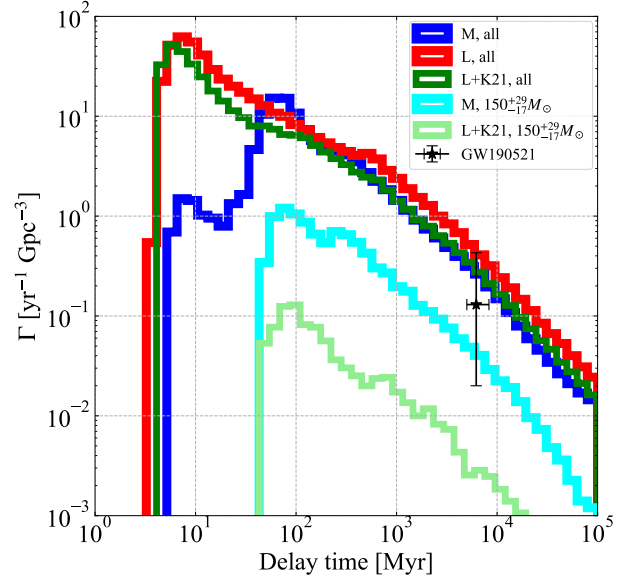


Figure 3. Merger rate density of Pop III BH-BHs in the M (blue), L (red), and L+K21 (green) models as a function of delay time. The light-blue and light-green curves indicate BH-BH mergers in the M and L+K21 models, where their total masses are within the error bar of the total mass of GW190521. There is no such BH-BH mergers in the L model. The delay time and rate of GW190521 are indicated by the star mark with error bars.

experience large mass loss through stable mass transfer or common envelope evolution. They lose their hydrogen envelopes and leave naked He stars. If the naked He stars have $45 - 65 M_{\odot}$ and $> 65 M_{\odot}$, they leave $45 M_{\odot}$ BHs and no remnants, respectively. They can leave only BHs with $\lesssim 45 M_{\odot}$. Thus, they cannot form GW190521-like BH-BHs. In the M model, stars with $M_{\text{zams}} = 50 - 90 M_{\odot}$ expand up to $\sim 10^2 R_{\odot}$, and keep blue-supergiant stars until they collapse to BHs. Such stars lose little mass through stable mass transfer, and tend not to experience common envelope evolution. They can maintain massive hydrogen envelopes. They can leave BHs with $50 - 90 M_{\odot}$ because their He core masses are $\lesssim 45 M_{\odot}$. Eventually, they can form GW190521-like BH-BHs. We discuss about the L+K21 model later.

We plot the delay time of GW190521 with error bars in Figure 3. We adopt $z = 0.82^{+0.28}_{-0.34}$ for the redshift of GW190521, and $0.13^{+0.30}_{-0.11} \text{ yr}^{-1} \text{ Gpc}^{-3}$ for its rate, as presented in Table 1. The rate of BH-BHs with total masses of $150^{+29}_{-17} M_{\odot}$ in the M model is slightly smaller than the median value of the rate of GW190521-like events, and within the error bars of 90% credible intervals. Our Pop III formation model is pessimistically small; therefore our rate can be regarded as the lower limit. Thus, a Pop III binary can be the origin of GW190521, if the M model can apply for Pop III stars. In contrast, if Pop III stars evolve along with the L model, no Pop III binary can form GW190521-like events.

Figure 4 shows the mass distributions of BH-BHs in the M, L, and L+K21 models (see Appendix B to quantify their numerical noise). We define the averaged merger rate density $\bar{\Gamma}$ over the error bar of the delay time of GW190521 as follows:

$$\bar{\Gamma} = \frac{1}{t_{d,f} - t_{d,i}} \int_{t_{d,i}}^{t_{d,f}} \Gamma dt_d, \quad (2)$$

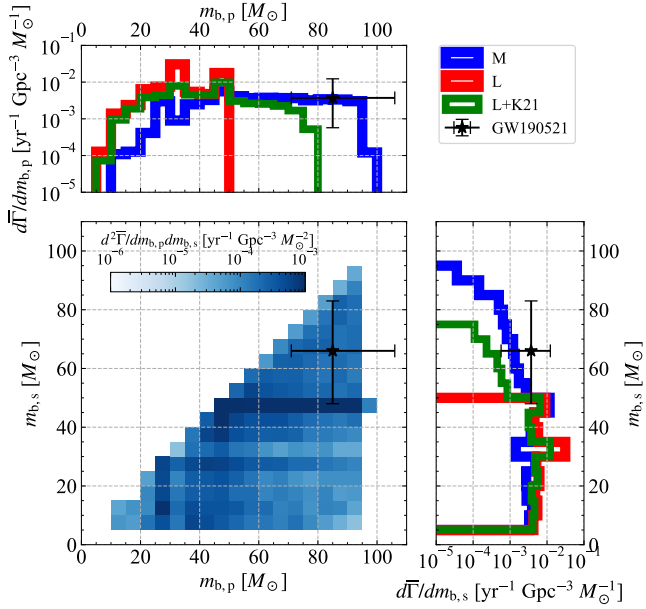


Figure 4. Mass distribution of the merging BH-BHs at the redshift of the GW190521 event in the M (blue), L (red), and L+K21 (green) models. The $\bar{\Gamma}$ is defined in the main text, and $m_{b,p}$ and $m_{b,s}$ are the primary and secondary BH masses respectively, where $m_{b,p} \geq m_{b,s}$. The 2D histogram indicates just the M model. The mass and rate of GW190521 are indicated by the star marks with error bars. In order to obtain the rate per mass of GW190521, we divide the rate of GW190521 by the widths of error bars of the BH masses, assuming that the rate is distributed uniformly in the error bars of the BH masses.

where we adopt $t_{d,i} = 5.5$ Gyr and $t_{d,f} = 8.8$ Gyr. To investigate the BH-BH mass distribution, we differentiate the averaged merger rate by the primary BH mass $m_{b,p}$ or secondary BH mass $m_{b,s}$, where $m_{b,p} \geq m_{b,s}$. The maximum masses of the primary and secondary BHs are $\sim 50 M_{\odot}$ in the L model. This is because of combinations of common envelope evolution and PPI effects as described above. In contrast, the maximum masses of the primary and secondary BHs are $\sim 100 M_{\odot}$ in the M model. The maximum masses are roughly determined by the maximum BH mass obtained through single star evolution, $\sim 95 M_{\odot}$ (Figure 2). The maximum BH mass obtained through binary star evolution is larger than obtained through single star evolution. This reason is explained as follows. A binary system containing a $95 M_{\odot}$ star as a secondary star. This star evolves to a post-MS star without binary interaction. Its He core mass is $< 45 M_{\odot}$. When it is a post-MS star, it gets extra mass through stable mass transfer from its companion star, and grows to a post-MS stars with $\sim 100 M_{\odot}$. Its He core mass does not increase through stable mass transfer because it is a post-MS star. Thus, it collapses to form a $\sim 100 M_{\odot}$ BH.

We focus on the results obtained using the L+K21 model. As seen in Figures 3 and 4, GW190521-like BH-BHs are formed in the L+K21 model despite that stars partially evolve along with the L model. Further, we describe the formation mechanism of BH-BHs with the maximum BH mass of $\sim 80 M_{\odot}$, similar to GW190521. A star with $M_{zams} \sim 90 M_{\odot}$ raises its He core with $\lesssim 45 M_{\odot}$ when it enters into the post-MS phase. Subsequently, it expands to $\geq 10^3 R_{\odot}$, and starts stable mass transfer at a certain time. The stable mass transfer increases M_c/M_t of the post-MS star. When its M_c/M_t becomes

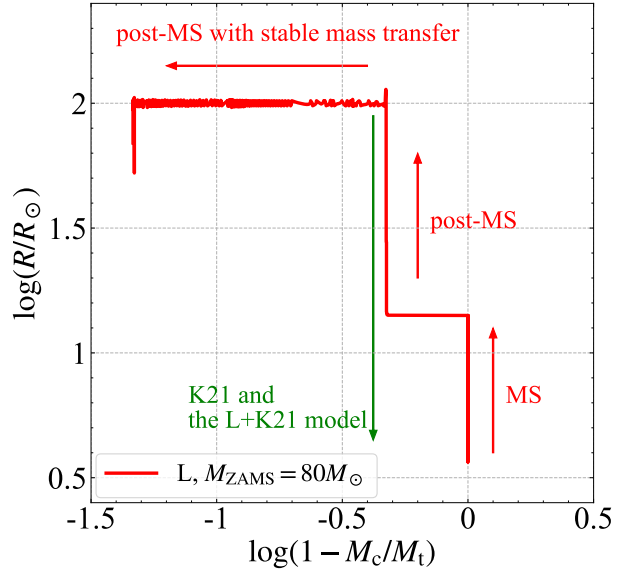


Figure 5. Radius evolution of a star with $M_{zams} = 80 M_{\odot}$ in the L model with the He core mass fraction (M_c/M_t). We model the stable mass transfer such that the star loses its mass when it exceeds $10^2 R_{\odot}$. The star has no He core in the MS phase; thus, $M_c/M_t = 0$ initially. In the post-MS phase, the star first expands freely up to $10^2 R_{\odot}$. Subsequently, the star loses its mass through stable mass transfer, and maintains its radius $10^2 R_{\odot}$ until $M_c/M_t \sim 0.95$. This means that $q_{He,crit} \sim 0.95$ is correct for this star. If $q_{He,crit} = 0.58$ were correct, the star would shrink to its He core size at $M_c/M_t = 0.58$, as indicated by the green arrow.

larger than $q_{He,crit} (= 0.58)$ (i.e. $M_c/M_t > q_{He,crit}$), it suddenly shrinks to its He core size, and stops the stable mass transfer. It does not lose its mass until it collapses to a BH. Its He core mass is $\lesssim 45 M_{\odot}$; thus, it can avoid PPI and PISN, and can directly collapse to form a BH with $\sim 45 q_{He,crit}^{-1} M_{\odot}$, which is equal to $78 M_{\odot}$. The maximum BH mass is also consistent with the result of K21.

The comparison between the L and L+K21 models clearly shows that the K21's modeling of post-MS stellar radii plays an important role in forming GW190521-like BH-BHs. We examined whether $q_{He,crit} = 0.58$ can be applicable to Pop III stars with $M_{zams} = 60 - 90 M_{\odot}$ in the L model. We prepared a Pop III star with $M_{zams} = 80 M_{\odot}$, which can leave a BH in the PI MG if it maintains its hydrogen envelope. The star evolves in the L model by the HOSHI code, a 1D stellar evolution code (Takahashi et al. 2016, 2018, 2019; Yoshida et al. 2019). The star experiences mass loss through stable mass transfer so as not to exceed $10^2 R_{\odot}$. Figure 5 shows its radius evolution. When the star enters into the post-MS phase, its He core mass (M_c) is about half the total mass (M_t). The star exceeds $10^2 R_{\odot}$ at a certain time in the post-MS phase. Subsequently, it loses its hydrogen envelope, and M_c/M_t increases. We can see that the star keeps its radius $10^2 R_{\odot}$ until $M_c/M_t \sim 0.95$. When its M_c/M_t exceeds 0.95, the star suddenly shrinks. This results mean $q_{He,crit} \sim 0.95$ and are in favor of $q_{He,crit} \sim 0.99$, i.e. the L model. In contrast, K21 have modeled the response of a stellar radius, such that a star shrinks down to its He core radius ($\sim 1 R_{\odot}$) when $M_c/M_t = 0.58$ as indicated by the green arrow in Figure 5. This result shows that $q_{He,crit} = 0.58$ is not applicable to a Pop III star with $M_{zams} = 80 M_{\odot}$ in the L model.

In summary, Pop III binary systems in the M model (a model with a small convective overshoot parameter) can form BH-BHs in the lower half of the PI MG (65 – 100 M_{\odot}). Consequently, BH-BHs in the M model also cover well the error range of the masses of GW190521. In contrast, BH-BHs in the L model (a model with a large convective overshoot parameter) cannot form the mass combination of GW190521. In the L+K21 model, Pop III binary systems can form GW190521-like BH-BHs because of their $q_{\text{He,crit}}$. However, their $q_{\text{He,crit}}$ is not applicable to a Pop III stars with $M_{\text{zams}} = 80 M_{\odot}$ which form BHs in the PI MG.

4 SUMMARY AND DISCUSSION

We perform BPS calculations, adopting the M and L models for Pop III star evolution models, where the M and L models have small and large convective overshoot parameters. The M model is similar to the F21’s model, and the L model is the same as the T21’s model. Additionally, we treat the L+K21 model similar to the K21’s model.

In the M model, Pop III binary systems can form GW190521-like BH-BHs. Stars in the M model maintain small radii until they experience supernovae or direct collapse to BHs, and tend not to interact with their companion stars. Finally, they can leave BHs in the lower half of the PI MG (65 – 100 M_{\odot}) through binary evolution. The merger rate of BH-BHs in the lower half of the PI MG is $4 \times 10^{-2} \text{ yr}^{-1} \text{ Gpc}^{-3}$ even in a pessimistic Pop III formation model. This is comparable to the merger rate of GW190521-like BH-BHs. Consequently, Pop III binary systems can be the origin of GW190521 if the M model can apply to Pop III star evolution. This result is consistent with the F21’s results.

In the L model, Pop III binary systems cannot form GW190521-like BH-BHs. Stars expand up to $\gtrsim 10^3 R_{\odot}$, and actively interact with their companion stars. They lose their hydrogen envelopes through stable mass transfer or common envelope evolution, and become naked He stars. Finally, they leave BHs with $\sim 45 M_{\odot}$ at most. Thus, the choice of a convective overshoot parameter strongly affects the formation of GW190521-like BH-BHs. We cannot conclude that the origin of GW190521 is a Pop III binary because determining the correct overshooting parameter is highly uncertain.

In the L+K21 model, GW190521-like BH-BHs are also formed because of their $q_{\text{He,crit}}$. However, their $q_{\text{He,crit}}$ is not reasonable for a Pop III star with $M_{\text{zams}} = 80 M_{\odot}$ that form BHs in the PI MG.

Furthermore, we cannot also claim that the presence of GW190521 proves the correctness of a model with a small convective overshoot parameter (the M model) because there are many formation scenarios of GW190521, which are described in section 1. We expect future GW observations to determine if a Pop III binary system can be the origin of GW190521. Clearly, Pop III binary systems cannot form the upper half of the PI MG (100–135 M_{\odot}) through pure binary evolution even in a model with a small convective overshoot parameter (the M model), as shown in Figure 4. If the BH-BH merger rate is suddenly decreased from the lower half of the PI MG to the upper half of the PI MG, a Pop III binary can be the origin of GW190521⁴. Other formation scenarios should have BH mass distributions with gradual decrease in the ascending order of BH masses rather than BH mass distributions with sudden decrease. These scenarios form BHs in the

⁴ Vink et al. (2021) have claimed that Pop II stars can also form BHs with $\leq 100 M_{\odot}$ if the convective overshoot is ineffective. If this is the case, we may not identify if the origin of GW190521 is Pop II or Pop III stars, even if the BH-BH merger rate is suddenly decreased from the lower half of the PI MG to the upper half of the PI MG.

PI MG through BH/star mergers or gas accretion; thus, there is no reason for such sudden decrease.

Figure 4 shows a peak of secondary BHs at $\sim 45 M_{\odot}$. This is because PPI sweeps BH progenitors with He core mass of 45–65 M_{\odot} to BHs with 45 M_{\odot} . It appears that a Pop III binary tends to leave a BH-BH with a BH in the lower half of the PI MG and a BH with $\sim 45 M_{\odot}$. However, stars experiencing PPI do not always leave BHs with $\sim 45 M_{\odot}$, and can leave BHs with $\sim 40 - 60 M_{\odot}$ in reality (Leung et al. 2019; Belczynski et al. 2020). Thus, we expect that a peak of secondary BHs around at $\sim 45 M_{\odot}$ should be more mild, and cannot be a clue to identify the origin of GW190521-like events.

ACKNOWLEDGMENTS

We are grateful to Alessandro A. Trani for checking our manuscript, and anonymous referee for many suggestions for improving this paper. This research was supported in part by Grants-in-Aid for Scientific Research (17H01130, 17H06360, 17K05380, 19K03907, and 20H05249) from the Japan Society for the Promotion of Science, and by University of Tokyo Young Excellent researcher program. We would like to thank Editage (www.editage.com) for English language editing.

DATA AVAILABILITY

Results will be shared on reasonable request to authors.

APPENDIX A: THE CRITICAL MASS FRACTION IN BSE

In this section, we show $q_{\text{He,crit}} \sim 0.99$ in SSE/BSE (Hurley et al. 2000, 2002, respectively). Hurley et al. (2000) describe the radius of a post-MS star with large M_c/M_t in section 6.3 of their study. A post-MS star with large M_c/M_t has $\mu < 1$, where μ is defined as follow:

$$\mu = \left(1 - \frac{M_c}{M_t}\right) \min \left\{ 5.0, \max \left[1.2, \left(\frac{L}{7 \times 10^4 L_{\odot}} \right)^{-0.5} \right] \right\}. \quad (\text{A1})$$

The radius of this type of post-MS star is expressed as follows:

$$R = R'_c \left(\frac{R'}{R'_c} \right)^{\rho} \quad (\text{A2})$$

$$\rho = (1 + c^3) \frac{(\mu/c)^3}{1 + (\mu/c)^3} \mu^{0.1/\ln(R'/R'_c)} \quad (\text{A3})$$

$$c = 0.006 \max \left(1, \frac{2.5 M_{\odot}}{M_t} \right), \quad (\text{A4})$$

where R' is the radius of a post-MS star with $\mu \geq 1$ and R'_c is the radius of a post-MS star without hydrogen envelope. Eqs. (A1), (A2), (A3), and (A4) correspond to Eqs. (97), (100), (102), and (104), respectively. Note that these notations are different from those used by Hurley et al. (2000).

Eq. (A2) presents $R \rightarrow R'_c$ for $\rho \rightarrow 0$. Let us consider how ρ decreases with decrease in μ . $M_t > 10 M_{\odot}$ for our case; thus, $c = 0.006$, and $(1 + c^3) \sim 1$. Furthermore, $R'/R'_c \sim 10^2 - 10^4$, $0.1/\ln(R'/R'_c) \lesssim 0.02$, and thus, $\mu^{0.1/\ln(R'/R'_c)} \sim 1$ for $\mu \sim c$. In contrast, $(\mu/c)^3/[1 + (\mu/c)^3] \gtrsim 0.999$ for $\mu \gtrsim 10c$, and $(\mu/c)^3/[1 + (\mu/c)^3] \sim 0.5$ for $\mu \sim c$. Consequently, ρ suddenly decreases for $\mu \sim c$. The min term in Eq. (A1) is equal to 1.2 for our case; thus, $M_c/M_t \sim 0.95$ and 0.995 for $\mu \sim 10c$ and c , respectively. Therefore, we can see $q_{\text{He,crit}} \sim 0.99$ in BSE.

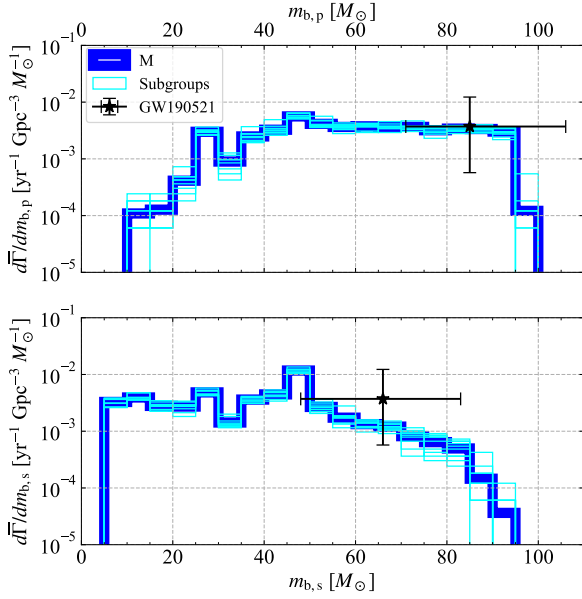


Figure B1. Mass distribution of the merging BH-BHs at the redshift of the GW190521 event in the M model and its 10 subgroups. The upper and lower panels correspond to the upper and right panels of Figure 4, respectively. The thick blue curves and star marks with error bars are the same as those shown in Figure 4.

APPENDIX B: NUMERICAL NOISE OF BPS CALCULATIONS

We estimated the numerical noise of BPS calculations by the jackknife resampling. We obtained 10 subgroups, dividing 10^6 binary systems into 10 equal parts. Subsequently, we investigated the difference in BH-BH properties among the 10 subgroups of 10^6 binary systems in the M model. Figure B1 shows the mass distributions of BH-BHs in the M model and its subgroups. We can see that the difference of mass distributions among these subgroups is the thickness of the blue curves for $25 \lesssim m_{b,p}/M_\odot \lesssim 95$ and $m_{b,s}/M_\odot \lesssim 85$. For other mass ranges, the numerical noise is a bit large because the number of merging BH-BHs is small in BPS calculations. Nevertheless, the numerical noise is negligible when we compare our results with GW190521.

REFERENCES

Abbott B. P., et al., 2016, *Physical Review Letters*, **116**, 061102
 Abbott B. P., et al., 2019a, *Physical Review X*, **9**, 031040
 Abbott B. P., et al., 2019b, *ApJ*, **882**, L24
 Abbott R., et al., 2020a, arXiv e-prints, p. arXiv:2010.14527
 Abbott R., et al., 2020b, *Phys. Rev. D*, **102**, 043015
 Abbott R., et al., 2020c, *Phys. Rev. Lett.*, **125**, 101102
 Abbott R., et al., 2020d, *ApJ*, **896**, L44
 Abbott R., et al., 2020e, *ApJ*, **900**, L13
 Anagnostou O., Trenti M., Melatos A., 2020, arXiv e-prints, p. arXiv:2010.06161
 Barkat Z., Rakavy G., Sack N., 1967, *Phys. Rev. Lett.*, **18**, 379
 Belczynski K., 2020, *ApJ*, **905**, L15
 Belczynski K., et al., 2016, *A&A*, **594**, A97
 Belczynski K., et al., 2020, *A&A*, **636**, A104
 Bond J. R., Arnett W. D., Carr B. J., 1984, *ApJ*, **280**, 825

Brott I., et al., 2011, *A&A*, **530**, A115
 Bustillo J. C., et al., 2021, *Phys. Rev. Lett.*, **126**, 081101
 Costa G., Bressan A., Mapelli M., Marigo P., Iorio G., Spera M., 2021, *MNRAS*, **501**, 4514
 De Luca V., Desjacques V., Franciolini G., Pani P., Riotto A., 2021, *Phys. Rev. Lett.*, **126**, 051101
 Di Carlo U. N., Mapelli M., Bouffanais Y., Giacobbo N., Santoliquido F., Bressan A., Spera M., Haardt F., 2020, *MNRAS*, **497**, 1043
 Ekström S., et al., 2012, *A&A*, **537**, A146
 El Eid M. F., Langer N., 1986, *A&A*, **167**, 274
 Farmer R., Renzo M., de Mink S. E., Fishbach M., Justham S., 2020, *ApJ*, **902**, L36
 Farrell E., Groh J. H., Hirschi R., Murphy L., Kaiser E., Ekström S., Georgy C., Meynet G., 2021, *MNRAS*, **502**, L40
 Fishbach M., Holz D. E., 2020, *ApJ*, **904**, L26
 Fragione G., Loeb A., Rasio F. A., 2020, *ApJ*, **902**, L26
 Fraley G. S., 1968, *Ap&SS*, **2**, 96
 Fryer C. L., Woosley S. E., Heger A., 2001, *ApJ*, **550**, 372
 Fryer C. L., Belczynski K., Wiktorowicz G., Dominik M., Kalogera V., Holz D. E., 2012, *ApJ*, **749**, 91
 Gayathri V., et al., 2020, arXiv e-prints, p. arXiv:2009.05461
 Graham M. J., et al., 2020, *Phys. Rev. Lett.*, **124**, 251102
 Heger A., Woosley S. E., 2002, *ApJ*, **567**, 532
 Hirano S., Hosokawa T., Yoshida N., Umeda H., Omukai K., Chiaki G., Yorke H. W., 2014, *ApJ*, **781**, 60
 Hurley J. R., Pols O. R., Tout C. A., 2000, *MNRAS*, **315**, 543
 Hurley J. R., Tout C. A., Pols O. R., 2002, *MNRAS*, **329**, 897
 Inayoshi K., Kashiyama K., Visbal E., Haiman Z., 2016, *MNRAS*, **461**, 2722
 Inayoshi K., Hirai R., Kinugawa T., Hotokezaka K., 2017, *MNRAS*, **468**, 5020
 Kinugawa T., Inayoshi K., Hotokezaka K., Nakauchi D., Nakamura T., 2014, *MNRAS*, **442**, 2963
 Kinugawa T., Nakamura T., Nakano H., 2020, *MNRAS*, **498**, 3946
 Kinugawa T., Nakamura T., Nakano H., 2021a, *MNRAS*, **501**, L49
 Kinugawa T., Nakamura T., Nakano H., 2021b, *Progress of Theoretical and Experimental Physics*, **2021**, 021E01
 Leung S.-C., Nomoto K., Blinnikov S., 2019, *ApJ*, **887**, 72
 Liu B., Bromm V., 2020a, *MNRAS*, **495**, 2475
 Liu B., Bromm V., 2020b, *ApJ*, **903**, L40
 Magg M., Klessen R. S., Glover S. C. O., Li H., 2019, *MNRAS*, **487**, 486
 Mangiagli A., Bonetti M., Sesana A., Colpi M., 2019, *ApJ*, **883**, L27
 Mapelli M., Santoliquido F., Bouffanais Y., Arca Sedda M., Giacobbo N., Artale M. C., Ballone A., 2020a, arXiv e-prints, p. arXiv:2007.15022
 Mapelli M., Spera M., Montanari E., Limongi M., Chieffi A., Giacobbo N., Bressan A., Bouffanais Y., 2020b, *ApJ*, **888**, 76
 Marigo P., Girardi L., Chiosi C., Wood P. R., 2001, *A&A*, **371**, 152
 Moffat J. W., 2020, arXiv e-prints, p. arXiv:2009.04360
 Palmese A., Conselice C. J., 2020, arXiv e-prints, p. arXiv:2009.10688
 Palmese A., Fishbach M., Burke C. J., Annis J. T., Liu X., 2021, arXiv e-prints, p. arXiv:2103.16069
 Paxton B., et al., 2013, *ApJS*, **208**, 4
 Podsiadlowski P., 1992, *PASP*, **104**, 717
 Renzo M., Cantiello M., Metzger B. D., Jiang Y. F., 2020, *ApJ*, **904**, L13
 Rice J. R., Zhang B., 2021, *ApJ*, **908**, 59
 Rodriguez C. L., Zevin M., Amaro-Seoane P., Chatterjee S., Kremer K., Rasio F. A., Ye C. S., 2019, *Phys. Rev. D*, **100**, 043027
 Romero-Shaw I., Lasky P. D., Thrane E., Calderón Bustillo J., 2020, *ApJ*, **903**, L5
 Roupas Z., Kazanas D., 2019, *A&A*, **632**, L8
 Safarzadeh M., Haiman Z., 2020, *ApJ*, **903**, L21
 Sakstein J., Croon D., McDermott S. D., Straight M. C., Baxter E. J., 2020, *Phys. Rev. Lett.*, **125**, 261105
 Sanyal D., Langer N., Szécsi D., -C Yoon S., Grassitelli L., 2017, *A&A*, **597**, A71
 Sharda P., Federrath C., Krumholz M. R., 2020, *MNRAS*, **497**, 336
 Skinner D., Wise J. H., 2020, *MNRAS*, **492**, 4386
 Susa H., Hasegawa K., Tominaga N., 2014, *ApJ*, **792**, 32
 Tagawa H., Haiman Z., Kocsis B., 2020, *ApJ*, **898**, 25

- Takahashi K., 2018, *ApJ*, **863**, 153
- Takahashi K., Yoshida T., Umeda H., Sumiyoshi K., Yamada S., 2016, *MNRAS*, **456**, 1320
- Takahashi K., Yoshida T., Umeda H., 2018, *ApJ*, **857**, 111
- Takahashi K., Sumiyoshi K., Yamada S., Umeda H., Yoshida T., 2019, *ApJ*, **871**, 153
- Tanikawa A., Yoshida T., Kinugawa T., Takahashi K., Umeda H., 2020, *MNRAS*, **495**, 4170
- Tanikawa A., Susa H., Yoshida T., Trani A. A., Kinugawa T., 2021, *ApJ*, **910**, 30
- The LIGO Scientific Collaboration et al., 2020, arXiv e-prints, p. [arXiv:2010.14533](https://arxiv.org/abs/2010.14533)
- Umeda H., Nomoto K., 2002, *ApJ*, **565**, 385
- Umeda H., Yoshida T., Nagele C., Takahashi K., 2020, *ApJ*, **905**, L21
- Vink J. S., Higgins E. R., Sander A. A. C., Sabhahit G. N., 2021, *MNRAS*, **504**, 146
- Webbink R. F., 1984, *ApJ*, **277**, 355
- Yang Y., et al., 2019, *Phys. Rev. Lett.*, **123**, 181101
- Yoon S. C., Dierks A., Langer N., 2012, *A&A*, **542**, A113
- Yoshida T., Umeda H., Maeda K., Ishii T., 2016, *MNRAS*, **457**, 351
- Yoshida T., Takiwaki T., Kotake K., Takahashi K., Nakamura K., Umeda H., 2019, *ApJ*, **881**, 16
- de Souza R. S., Yoshida N., Ioka K., 2011, *A&A*, **533**, A32

This paper has been typeset from a $\text{\TeX}/\text{\LaTeX}$ file prepared by the author.